Research Square

Preprints are preliminary reports that have not undergone peer review.
They should not be considered conclusive, used to inform clinical practice,
or referenced by the media as validated information.

Eco-friendly synthesis of ZnO-nanoparticles using *Phoenix dactylifera L.* polyphenols: physicochemical, microstructural and functional assessment

JOHAR AMIN AHMED ABDULLAH (jabdullah@us.es)
Universidad de Sevilla https://orcid.org/0000-0002-5923-8254

Mercedes Jiménez-Rosado
Universidad de Sevilla Facultad de Química: Universidad de Sevilla Facultad de Quimica

Antonio Guerrero
Universidad de Sevilla Facultad de Química: Universidad de Sevilla Facultad de Quimica

Alberto Romero
Universidad de Sevilla Facultad de Química: Universidad de Sevilla Facultad de Quimica

Research Article

Keywords: Antioxidant activity, Antibacterial activity, Green synthesis, ZnO-Nanoparticles, Polyphenols

Posted Date: September 28th, 2022

DOI: https://doi.org/10.21203/rs.3.rs-1934475/v2

License: This work is licensed under a Creative Commons Attribution 4.0 International License.
Read Full License

Abstract

Recently, nanoparticles (NPs) synthesis has evolved into a green nanotechnology field, requiring more eco-synthesis of nanoparticles due to the high costs of other chemical-physical methods. Among the most commonly used nanomaterials, ZnO-NPs are highly valuable due to their specific, thermal, optical, and electronic features. Thus, the main objective of this work was to investigate the green synthesis of ZnO-NPs employing *Phoenix dactylifera L.* extract, which is rich in polyphenols, as a reducing agent. In this way, the effect of the concentration of both the precursors and the reducing agent was evaluated.The NPs were compared through X-ray diffraction (XRD), transmission electron microscopy (TEM), scanning electron microscopy (SEM) and Fourier infrared transformation spectroscopy (FTIR). Additionally, we evaluated the antioxidant properties (TAC and DPPH) and antibacterial activity of these nanoparticles against Gram-positive Staphylococcus aureus (S. aureus) and Gram-negative Escherichia coli (E. coli) pathogenic strains. The results show that it is possible to obtain ZnO-NPs using a green reducing agent (polyphenol extract), presenting a particle size between 18.1 and 61.6 nm. In addition, this synthesis highlighted the antioxidant and antibacterial activities of these nanoparticles. In conclusion, this method could be a suitable substitute for typical toxic methods for the synthesis of metallic nanoparticles.

1 Introduction

Interest in nanomaterials has increased due to the special characteristics that allow them to be applied in a wide range of fields and applications, being used in the chemical, medical, pharmaceutical, mechanical, and technological industries [1]. Almost all academic disciplines consider this to be one of the most prominent areas of research and development [2]. As a result, they have many unique characteristics, including strength, lightweight, excellent chemical reaction, very small size with high surface area and stability. Among the most commonly used nanomaterials, zinc oxide nanoparticles (ZnO-NPs) have gained considerable interest in scientific and medical communities [3]. It is a very valuable material with multiple properties suitable for high technology, such as light-emitting diodes, optical detectors, chemical and biological sensors, energy aggregators (e.g., solar cells), nano-molders and electromagnetics. This is due to their highly attractive chemical properties such as high electrochemical correlation coefficient and high photochemical stability, as well as their excellent electronic, electrical, and physical properties [4]. ZnO-NPs have not only been used in these fields; they also play an important role in other fields, such as cosmetics and drug delivery, where they are widely used to treat various skin diseases due to their potential UV-ray absorption (e.g, as UV radiation deterrents in sunscreens), antimicrobials and many medical products [5,6]. On the other hand, nanoparticles can be tailored to be used against specific diseases, being of special interest in medicine, where they can provide new ways of treating diseases that are hard to target due to size constraints [7]. In addition, ZnO-NPs are considered safe and non-toxic according to the U.S. Food and Drug Administration, and they can be used in different medical-industrial sectors [8]. Furthermore, they are toxic to cancer cells, bacteria and leukemia cells, being attractive as drug delivery agents and gene delivery biosensors, as well as in cancer treatments [9]. It is safe to say that there have been no known human diseases caused by geometric nanoparticles [10].

Zinc oxide nanoparticles are scaled with a diameter smaller than 100 nm. The different manufacturing methods result in different physical and chemical properties of ZnO-NPs [11]. There are several methods to produce zinc oxide nanoparticles: sedimentation processes, hydrothermal methods, laser excision molecules, sol-gel methods, electrochemical deposits, chemical steam deposition, ultrasound, thermal decomposition, microwave-assisted combustion methods, combustion methods, two-step thermal-mechanical synthesis, precipitation, aluminium oxide coating, and electrical deposition using different solution concentrations, pH values, and washing media [12]. Nevertheless, these methods are costly and regrettably dependent on the use of toxic chemicals [13–15]. Thus, recently, many studies have focused on green ways to produce nanoparticles from noble metals that are simple, cost-effective, and repeatable [16]. The relevance of these green technologies is that they are cost-effective, non-toxic, rapid, and lead to high crystallinity at nanoparticle formations in a variety of sizes and shapes [17]. To develop ecologically safe technologies, mostly plant or fruit extracts are utilized [18]. They contain high concentrations of polyphenols, which reduce the metal salts into high-purity nanoparticles through their unique features (reducing properties, hydrogen bonding ability, nucleophilic nature, polarizability, acidity, chelating properties, etc.) [19]. These properties have led to the production of nanoparticles, thanks to their mentioned properties and suitable biocompatibility, and they have been thus vastly employed in biomedical applications [20–22].

Date palm (*Phoenix dactylifera L.*) is an ancient tropical and subtropical fruit plant that belongs to the Aceraceae family and is grown in the Arabian Peninsula (Yemen, Oman, Qatar, Saudi Arabia, the United Arab Emirates (UAE), Kuwait, as well as the southern regions of Jordan and Iraq), and Northern Africa (Egypt, Sudan, Libya, Tunisia and Algeria) [23–25]. *Phoenix dactylifera L.* provides food, medicine, construction materials and fuel, hence its name, the tree of life. It is an extremely widespread tree with a wide range of nutritional, economic, and medicinal applications, including food additives, antimicrobials, antilipidemic and anti-diabetes drugs [19,24] *Phoenix dactylifera L.* has previously been investigated for its high levels of phytochemicals (e.g., polyphenols, flavonoids, aldehydes, terpenoids, fatty acids alkaloids, etc.) [26–28]. A number of metal oxide nanoparticles have been synthesized using this plant species, such as iron oxide, gold, silver, nickel nanoparticles, etc. [24,29].

This study aimed to investigate the green synthesis of ZnO-NPs employing *Phoenix dactylifera L.* extract rich in polyphenols as a reducing agent. In this way, the effect of both precursor and reducing agent concentrations was evaluated. The further investigation involved X-ray diffraction (XRD), transmission electron microscopy (TEM), scanning electron microscopy (SEM) and Fourier infrared transformation spectroscopy (FTIR). Furthermore, the antioxidant (TAC and DPPH) and antibacterial (S. aureus and E. coli) activity of these nanoparticles were compared.

2 Materials And Methodology

Materials

Zinc chloride ($ZnCl_2$), methanol (CH_3OH), Ethanol (CH_3CH_2OH), sulfuric acid (H_2SO_4), sodium phosphate (Na_2HPO_4), ammonium molybdate ($(NH_4)_3PMo_{12}O_{40}$), gallic acid ($C_7H_6O_5$), hydrochloric acid (HCl), 2,2-diphenyl-1-picrylhydrazyl (DPPH), dimethyl sulfoxide anhydrous (DMSO) 99.9% (C_2H_6SO) were purchased from Sigma Aldrich (Darmstadt, Germany). Throughout the study, only analytical-grade chemicals and reagents were used.

Phoenix Dactylifera L. leaves were harvested from Seville (Spain), at an average temperature of 19±4 ºC (with maximum and minimum temperatures of 36 ºC and 6 ºC, respectively), at an average RH (relative humidity) of 53% (according to the NOAA; National Oceanic and Atmospheric Administration). Then, it was left to dry in the shade for 44 days at a mean temperature of 22±3 °C and an average RH of 35%.

Phoenix dactylifera L. extraction was performed according to previous studies with modifications [29,30]. Briefly, 30 g of powdered *Phoenix dactylifera L.* was extracted using distilled water (300 mL) through Soxhlet extraction at 98 °C for 8 h. The extraction yield was 53.8±0.8 % corresponding to 38.6±1.7 (mg GAE/g extract) of total polyphenol content (TPC). The extraction yield and TPC calculation are more detailed in a previous study [30].

Nanoparticles synthesis

ZnO-NPs synthesis was performed according to previous studies with modifications [29,30]. Briefly, 20 mL of the extract was transferred dropwise into 20 mL of zinc chloride ($ZnCl_2$) solution. Three different concentration ratios ([2:1], [1:1] and [1:2]) for the concentrations (0.1, 0.2, 0.4, 0.5, 1 and 2 M) were paired and evaluated. The resulting solutions were then transferred into beakers, heated at 50 °C under stirring for 2 h, and then purified by filtering through Whatman nº 1 papers and washing with distilled water at least three times to remove dirt and particles suspended in the mix. The samples were pretreated in an oven at 100 ºC for 8 hours, followed by a final heat treatment at 500 °C for 5 h to remove any residual material from the sample.

ZnO-NPs characterization

X-ray diffraction (XRD)

XRD pattern was obtained using a Brand diffractor (Bruker Model D8 advance A25 with Cu anode) to confirm the presence of crystalline phases in the sample. The crystalline size of ZnO-NPs and the crystallinity degree were calculated by applying the Debye-Scherrer formula, following the description in previous studies [29,31]. The diffractograms were obtained in the range of 2q (º) = 15-70.

Transmission electron microscopy (TEM)

The TEM study was performed to determine the crystalline characteristics of the nanoparticles, as well as their size. It was carried out using a Talos S200 microscope (FEI, USA) at 200 kV. Elemental information of the ZnO-NPs was labelled using Image-J free software [32].

Scanning electron microscopy (SEM)

SEM was primarily used to gather the size (average diameter distribution) and the structural morphology of the ZnO-NPs. This was carried out at an acceleration voltage of 10 kV using a Zeiss EVO scanning electron microscope (USA). To compare the samples, they were scanned at various magnifications. Image-J free software was used to label elemental information of the ZnO-NPs [32].

Fourier transform infrared spectroscopy (FTIR)

The vibration modes of the bonds present in the ZnO-NPs from 4000 to 400 cm^{-1} were used to gather information on the nanoparticles (NPs) structure using the FTIR spectrometer (Hyperion 100 Spectrometer, Bruker, USA). The spectrometer was configured in transmittance mode using a DTGS-KBr sensor. It is possible to identify three distinct zones at the global level: absorbance bands associated with alkyl chains on the surface (3000-2800 cm^{-1}), the COO- group in oleates (1800-900 cm^{-1}), and the Zn-O bonds in Zn-O (800-400 cm^{-1}) [33].

Antioxidant activity (TAC and DPPH)

The antioxidant activity was determined either through the products of oxidation or by the capacity of the reaction models to trap radicals. Two different tests have been used: the total antioxidant activity of phosphomolybdate (TAC) and the free radical scavenging of the DPPH test.

The TAC analyzes oxidation compounds, thereby searching for functional groups in derivatives of the original constituents (carbonyl compounds of aldehydes, ketones, dicarbonyls, etc.). The DPPH test determines how many radicals are trapped in relation to the amount of antioxidants applied.

The TAC and DPPH tests were carried out using the protocol described in a previous study without modifications [29]. Briefly, for TAC analysis, 2 mL of Zn-NPs (dispersed in HCl) was mixed with 2 mL of reagent (0.6 M H_2SO_4, 28 mM Na_2HPO_4 and 4 mM $(NH_4)_3PMo_{12}O_{40}$). Then, the mixture was incubated in a water bath at 95 °C for 90 min. The absorbance was read at 695 nm using spectrophotometry, gallic acid was used as a reference. The DPPH test was conducted by mixing 2 mL of ZnO-NPs/DMSO solution dispersed in different concentrations (0.125, 0.25, 0.5, 1, 2, and 4 mg/mL) with 2 mL of DPPH methanolic solution. After incubating the mixtures for 0.5 hours, the absorbance at 517 nm was determined. A mixture of DPPH and DMSO was used as a control. The inhibition percentage *IP (%)* of tested samples was calculated according to Equation (1)

$$IP(\%) = \left(\frac{A_D - A_{Da}}{A_D}\right) \cdot 100 \qquad (1)$$

Where A_D is the absorbance value of the oxidized solution (without ZnO-NPs antioxidant agent) and A_{Da} is the absorbance after adding ZnO-NPs antioxidant agent. Moreover, the IC_{50} (the necessary antiradical concentration to inhibit 50% of DPPH) was conducted using GraphPad Prism 9 software (Windows GraphPad Prism, 9.0.0, San Diego, California, USA, www.graphpad.com) [29].

Antibacterial activity

The antimicrobial activity of the as selected ZnO-NPs (optimized through TAC and DPPH values) was evaluated using an agar diffusion experiment as described by Behera et al. with slight modification [34]. In this way, holes of 9 mm of diameter were made in agar gels inoculated with *Staphylococcus aureus* (S. aureus) and *Escherichia coli* (E. coli) using the end of a cone-shaped micropipette tip as a perforator. After that, the holes were filled with 20 µL (50 mg/mL) of ZnO-NPs dispersed in distilled water (using ultrasound for 20 min). 10 µL of Gentamicin (50 µg/mL) in wells of 2 mm of diameter was used as standard.

The antibacterial activity was assessed by measuring the inhibition diameters surrounding the ZnO-NPs solution after 24 and 48 h of incubation at 37°C using Image-J software [35].

Statistical analysis

GraphPad Prism9 and IBM SPSS Statistics 26 software were used for statistical analysis. One-way ANOVA was applied to estimate the significance of the differences between observations. At least three replicates of the data were used to calculate the mean ± SD. The significance level was estimated using the HSD Tukey statistical analysis ($p < 0.05$).

3 Results And Discussion

XRD

The X-ray diffractograms of ZnO-NPs synthesized by the *Phoenix dactylifera L.* extract using different concentrations are depicted in Figure 1.

The peaks observed at 2θ (º) = 31.7, 34.4, 36.3, 47.5, 56.6, 62.9, 66.4, 67.9 and 69.1 could be attributed to the crystallographic reflection's planes (100), (002), (101), (102), (110), (103), (200), (112), and (201), deriving from the hexagonal structure of the zinc oxide; space group: P63mc (186) with standard

crystallographic parameter a = 3.2501 Å b = 3.2501 Å, c =5.2071 Å (JCPDS nº.01-079-2205 standard zincite ZnO powder diffraction pattern) [36].

The well-defined and sharper peaks in the XRD of ZnO-NPs reveal that the ZnO-NPs exhibit varying levels of crystallinity. The crystalline sizes and crystallinity degree calculated by the Debye-Scherrer equation are reported in Table 1. For the [1:2] and [2:1] ratios, nanoparticles size decreased at lower concentrations of both the precursor and the reducing agent (Table 1), possibly due to lower agglomeration or aggregation. Similar results reported by Kodama et al. showed aggregation when [OH] was high [37]. Green synthetic ZnO-NPs tended to be larger in size at higher concentrations of both precursor and extract reducing agent, which may be attributed to the competition between functional groups of the extract and zinc ions, thus the reduction rate would also increase [17]. This could indicate that the concentration of 0.1 M of the extract is just right for obtaining the lowest crystallite sizes. Similar results have been found in the literature [38–40]. For the [1:1] ratio, the size and number of nanoparticles increased with the precursor concentration. Similar results were obtained in other studies; for example, Fuad et al. found that the increase in the concentration of the precursor from 30 to 35 mM led to an increase in nanoparticle size from 44.6 to 58.9 nm [41]. Jon et al., who synthesized gold nanoparticles from *Zea Mays Extract* using chloroauric acid ($HAuC_{l4}$) as a precursor, found that the size of the nanoparticles increased from 6 to 50 nm with an increase in the precursor concertation from 0.5 to 5 mM [42]. Furthermore, the sizes of synthesized ZnO-NPs using *Phoenix dactylifera L.* in this study were much smaller than those obtained using other methods reported in the literature; for example, Mohammad et al., using the sol-gel process at three different ratios of 3:1, 1:1 and 1:3, obtained ZnO nanoparticle sizes of 160, 220 and 250 nm, respectively [43].

The synthesis mechanism for the ZnO nanoparticles is shown in Figure 2. *Phoenix dactylifera. L* extract, as a good source of polyphenols (phytochemicals), reduces metal precursors ($ZnCl_2$) to metal nanoparticles (ZnO-NPs). Polyphenols are non-toxic antioxidants that can reduce precursors and stabilize the obtained nanoparticles without generating toxic wastes [19,44]. Phenolic compounds, as essential phytochemicals, contribute to reducing processes. Thus, the concentration of these reducing agents (phenolic compounds) varies for different types of plant extracts. As a result, leaf extract concentration affects nanoparticle synthesis [45]. Studies propose that the metal ions after the reduction by phytochemicals may be covered in an organic compound in three phases for stabilization: i. Activation phase: consists of precursor formation, metal ion reduction (e.g., neutralization reactions) and metal ion nucleation; ii. Growth phase: contributes to nanoparticle stability; iii. Termination phase: determines the shape of nanoparticles, where ageing processes such as coarsening and aggregation take place [28,46,47].

Nucleation kinetics is correlated with chemical reaction kinetics and molecular mechanisms in this case. As a result of the colloidal green synthesis of ZnO from $ZnCl_2$ and R-OH (extract phenolic compounds) in water, the following chemical reaction can be described [47]:

$$n\mathrm{ZnCl_2} + 2n\mathrm{R\text{-}OH} + l\mathrm{H_2O} \rightarrow \mathrm{Zn^{2+}}_n(\mathrm{OH^-})_m(\mathrm{H_2O})_l\mathrm{Cl^-}_k + (2n - k)\ \mathrm{Cl^-} + (2n - m)\ \mathrm{OH^-} + 2n\mathrm{R^+} \rightarrow n\mathrm{ZnO} + (l + n)\ \mathrm{H_2O} + 2n\mathrm{R\text{-}Cl} \quad (2)$$

As can be seen, the zinc-ligand molecule acts as a nucleation precursor, with $2n = m + k$ when a zero-charge precursor is present. Precursor formation kinetics, which show a rapid behavior, increase the supersaturation with time and initiate a burst of nucleation if a certain threshold is reached. The supersaturation decreases in response to the relative velocities of precursor nucleation and the amount of the total material present in the system, which, in turn, delays and eventually stops the nucleation. When the precursor formation rate is slow, nucleation can take place at constant supersaturation for an extended time [47].

Plant polyphenols cause metals to form their metal oxides and make them reach the growth and stabilization phases. Finally, by binding metal ions to oxygen, nanoparticles with a defined shape are formed at the final treatment with the annealing temperatures [28,46].

Table 1 also shows the relationship between the crystallinity and the variation in the concentration ratio [precursor: extract reducing agent], which explains that the higher the percentage of the extract (reducing agent), the greater the crystallinity. This is due to the fact that ZnO-NPs at high concentrations (both precursor and extract reducing agent) generally form crystals containing more ZnO than at low concentrations [48].

TEM

Figure 3 shows TEM images of the synthesized ZnO-NPs with different morphologies and the histograms of nanoparticle size distributions, where they were fitted by applying a normal curve. Accordingly, nanoparticle average diameters ranged between 18.6±0.5, which corresponds to the system with the lowest content of precursor and reducing agent, and 61.6±1.3 nm, obtained for the highest concentration of both agents (Table 1).

As can be observed, the [2:1] ratio revealed numerous nanoparticle aggregates and cubic particles, which may indicate the competition between functional groups of the extract and zinc ions on the ZnO-NPs surface, and thus, the reduction rate would also increase [17]. For the [1:1] ratio, it showed weak aggregated, quasi-spherical, cubic, and hexagonal nanoparticles. When the ratio was inversed to [1:2] by doubling the extract concentration, the nanoparticles were better dispersed with different shapes, cubic, hexagonal and spherical structures. This indicates that the increase in reducing agent concentration (i.e. an increase in $-OH^-$) may produce a large number of zinc hydroxide , leading to ZnO-NPs formation, which in turn reduces the growth rate and the interaction between nanoparticles [49]. These results are similar to those of previous studies [38,50,51]. It would be worth trying to confirm these results with another microscopy technique such as SEM.

SEM

Figure 4 shows ZnO-NPs morphology and nanoparticles size distributions. Nanoparticles/nanorods presented an average diameter between 18.1±0.5 and 49.6±0.3 nm, from the lowest to the highest reactant contents. Their lengths ranged between 48 nm (for the 0.2:0.4 system) and 291 nm (for the 0.5:0.5 system) but showed a less regular dependence on the precursor or reducing agent concentrations. Detailed results are shown in Table 1.

For the [2:1] ratio, it was observed to show numerous closely packed and larger rod-shaped nanoparticles, with spherical, face-centered rhombohedral, cubic and hexagonal structures. When the ratio was adjusted to [1:1], it was observed to reveal numerous well-dispersed hexagonal nanorods at lower concentrations, and a few spherical nanoparticles at higher concentrations with slight aggregation/agglomeration. When the ratio was changed to [1:2] by doubling the extract concentration, excellently dispersed hexagonal nanorods were obtained, as well as cubic and spherical nanoparticles. Similar results have been reported in previous studies [17,37,41,48,52]. These polygonal or anisotropic structures indicate that the precursor and reducing agent concentrations affect nanoparticle sizes and morphologies. The interactions of nanoparticles with each other resulted in slight agglomeration of NPs in some cases [52,53], while in other cases they grew and agglomerated due to the phytochemicals in *Phoenix* extracts acting as stabilizing agents and the ageing effect caused by reflux conditions [53]. As a result of hydrogen bonding (H-bonding) in bioactive molecules, these nanoparticles had the appearance of aggregates [32,54,55]. It can be noticed that, in general, the nanoparticle sizes obtained from SEM are rather coincident with those obtained from the other two techniques applied (particularly from DRX).

FTIR

FTIR characterization of ZnO-NPs synthesized at different concentrations and concentration ratios are shown in Figure 5.

The first observation was focused on the area of 800-400 cm^{-1}, which characterizes Zn-O bonds. Peaks observed in the range of 650-400 cm^{-1} are caused by the Zn–O vibrations of ZnO-NPs [17,51]. As can be seen in the whole systems [2:1], [1:1] and [1:2], the low concentrations have led to an increase in absorbance, which may justify the smaller nanoparticles. Similar trends have shown that the shifting in absorbance and band area to be increased correlates with smaller particle sizes [56].

The biomolecules responsible for reducing the metal precursors to ZnO nanoparticles appear in the range of 3500-3200 cm^{-1}, and a band at 3416 cm^{-1} is attributable to the vibrational stretching of OH polyphenolic compounds of *Phoenix dactylifera L.* The bands around 1631.37, 1623.52, and 1635.29 cm^{-1} are attributable to the stretching vibration of C = C and bonds in alkene groups or to aromatic ring deformation, and those which appear around 1733, 1737, and 1741.1 cm^{-1} are assigned to – C=O bonds of aldehydes, ketones and esters, and the bands at 1376.47 1384.31, 1380,39 are associated with ester

groups [57,58]. The bands in the range of 1200 -1247 cm^{-1} could present an asymmetric stretching vibration of C–O, typical of polyphenolic compounds [58]. The bonds appearing in the range of 1039 -1070 cm^{-1} present C–O–C stretching vibration of phenolic compounds and polysaccharides [58]. The bonds in the range of 1105-1160 cm^{-1} are assigned to C–O–H in phenolic compounds [58]. The reduction of $ZnCl_2$ by the phenolic compound of *Phoenix dactylifera L.* into ZnO-NPs produced the absorption band around 1643 cm^{-1} to be segmented into three peaks at 1653, 1633 and 1623 cm^{-1} [29].

Antioxidant activity

Table 1 also summarizes the total antioxidant activity (TAC) and IC_{50} for the inhibition of 50% of free radical DPPH. A lower IC_{50} value presents a higher antioxidant activity.

For the ZnO-NPs synthesized at [2:1] and [1:1] ratios, they were observed to exhibit higher total antioxidant activity at lower concentrations (Table 1), which could be due to the small size of ZnO-NPs and the presence of capping agents [59]. Where the highest TAC of ZnO-NPs was generally observed to be produced with the ZnO-NPs at the [1:2] ratio (Table1). This could be explained by the simultaneous activity of phenolic compounds (phytochemicals) remaining as antioxidant agents and zinc ions in ZnO-NPs as catalysts by transferring a single electron and a hydrogen atom or by releasing an oxygen atom [53,60,61]. Further studies indicated that bioactive compounds of the extracts were adsorbed onto nanoparticles [62]. Furthermore, research has demonstrated that nanoparticles have a higher total antioxidant activity than the standard (gallic acid) [63]. For the anti-free radical DPPH activity, the optimum IC_{50} was attributed to the ZnO-NPs prepared at lower concentrations in each ratio system (Table 1), which may be due to the lower-size nanoparticles [64]. Nevertheless, larger ZnO-NPs had polygonal or anisotropic structures and, as a result, exhibited a lower specific surface area, which reduced their reactivity with DPPH radicals; similar trends have been reported by K. Zar Myint et al., 2021 and S. Pu et al., 2019 [64,65]. The ZnO-NPs synthesized using an eco-friendly *Phoenix dactylifera L* extract exhibited strong antioxidant activity. As a standard, the IC_{50} value for gallic acid was determined to be 0.4±0.2 mg/mL.

Antibacterial activity

Table 2 shows the inhibition areas of ZnO-NPs through their significant parameter (diameter). The results were comparable to those of Gentamicin (50 µg/mL). It was found that ZnO-NPs exhibited moderate antibacterial activity against pathogenic Gram-positive (S. aureus) and Gram-negative (E. coli) bacteria, with inhibition areas of up to 19 mm, as shown in Figure 6. The green synthesized ZnO-NPs with higher TAC presented a higher antibacterial activity than those with higher DPPH antiradical activity against both pathogenic strains. This could be due to the smaller size of the ZnO-NPs, which confers NPs an excellent ability to inhibit the replication of bacterial DNA [66,67]. Small nano-scale particles allow them to penetrate the bacterial membranes and inactivate them by zero-valent metal oxide nanoparticles

(ZVMON), which then could oxidize intercellular oxygen, causing oxidative stress and cell membrane damage. The oxidative stress might be produced by reactive oxygen species (ROS), such as hydroxyl radicals (–OH), hydrogen peroxide (H_2O_2), singlet oxygen ($^1O_2$) and superoxide radicals (O^{2-}) [22,68]. Bacteria are especially susceptible to ROS, which can damage their proteins and DNA. Both pathogenic bacteria (S. aureus and E. coli) were inhibited by ZnO-NPs investigated here, which could be a rich source of ROS. Similar reactions have been reported in the literature [69–71]. Nevertheless, the high antibacterial activity of ZnO-NPs could also be associated with their high crystallinity, which allows the released Zn^{+2} to collide with the negatively charged membranes of bacteria, thereby destroying their protein structure [72,73].

4 Concluding Remarks

The use of *Phoenix dactylifera L.* extract in the synthesis of ZnO-NPs provides an excellent route for an eco-friendly method of nanoparticle manufacture.

These nanoparticles appear to have a variety of shapes and structural features, and SEM examination revealed that nanoparticles were aggregating and forming networks depending on the concentration of both the precursor and the reducing agent used. ZnO-NPs synthesized from *Phoenix dactylifera L.* extract have been shown to have high antioxidant activity by trapping free radicals. Consequently, nanotechnology-based antioxidants are difficult to compare across different cases, and the antioxidant capacity of NPs varies according to their size, crystallinity degree, shape, and concentration. In the presence of spherical NPs, the antioxidant activity may be higher than in those systems with irregular or polygonal NPs. Therefore, ZnO-NPs synthesized from *Phoenix dactylifera L.* extract may be regarded as promising antibacterial drugs with great potential for the replacement of today's antibiotics.

The green synthesized ZnO-NPs through the use of eco-friendly *Phoenix dactylifera L.* extracts could be a potential substitute for NPs obtained by chemical methods due to a variety of benefits, related to process efficiency, cost-effectiveness and eco-friendliness, but also to its reactivity and functionality (antioxidant capacity and antibacterial activity)

Declarations

Acknowledgements

The authors would like to acknowledge the MCI/AEI/FEDER, EU project (Ref. RTI2018-097100-B-C21) that supports this work. In addition, the authors would also thank the predoctoral grant from Johar Amin Ahmed Abdullah (Universidad de Sevilla, CODE 810) and Mercedes Jiménez-Rosado (Ministerio de Educación y Formación Profesional, FPU17/01718). The authors also thank CITIUS for granting access to and their assistance with the DRX area characterization and microscopy services.

Ethic approval: Not applicable.

Consent to participate: Not applicable.

Consent to publish: Not applicable.

Author Contributions: Conceptualization, J.A.A.A., A.R. and A.G.; methodology, J.A.A.A. and M.J.R.; software, J.A.A.A.; validation, J.A.A.A., and A.R.; formal analysis, M.J.R.; investigation, J.A.A.A. and M.J.R.; resources, A.G.; data curation, J.A.A.A; writing—original draft preparation, J.A.A.A. and M.J.R.; writing—review and editing, A.R. and A.G.; visualization, A.R. and A.G.; supervision, A.R. and A.G.; project administration, A.G.; funding acquisition, A.G.

Competing interests: The authors declare no conflict of interest.

Data availability: The data presented in this study are available on request from the corresponding author.

References

1. Umadevi, M.; Bindhu, M.R.; Sathe, V. A Novel Synthesis of Malic Acid Capped Silver Nanoparticles using Solanum lycopersicums Fruit Extract. *J. Mater. Sci. Technol.* **2013**, *29*, 317–322, doi:10.1016/j.jmst.2013.02.002.

2. Paul, D.R.; Robeson, L.M. Polymer nanotechnology: Nanocomposites. *Polymer (Guildf).* **2008**, *49*, 3187–3204, doi:10.1016/j.polymer.2008.04.017.

3. Al-maamori, M.H. Preparation and Surface Modification of Zinc Oxide Nanoparticles. *J. Babylon Univ. J. Appl. Pure Sci.* **2017**, *25*, 497–503.

4. Kolodziejczak-Radzimska, A.; Jesionowski, T. Zinc oxide-from synthesis to application: A review. *Materials (Basel).* **2014**, *7*, 2833–2881, doi:10.3390/ma7042833.

5. Wahab, R.; Hwang, I.H.; Shin, H.-S.; Kim, Y.-S.; Musarrat, J.; Al-Khedhairy, A.A.; Siddiqui, M.A. Zinc Oxide Nanostructures and their Applications. In *Intelligent Nanomaterials*; John Wiley & Sons, Inc.: Hoboken, NJ, USA, 2012; pp. 183–212 ISBN 9780470938799.

6. Mirzaei, H.; Darroudi, M. Zinc oxide nanoparticles: Biological synthesis and biomedical applications. *Ceram. Int.* **2017**, *43*, 907–914, doi:10.1016/j.ceramint.2016.10.051.

7. Moezzi, A.; McDonagh, A.M.; Cortie, M.B. Zinc oxide particles: Synthesis, properties and applications. *Chem. Eng. J.* **2012**, *185–186*, 1–22, doi:10.1016/j.cej.2012.01.076.

8. Al-Mohaimeed, A.M.; Al-Onazi, W.A.; El-Tohamy, M.F. Multifunctional Eco-Friendly Synthesis of ZnO Nanoparticles in Biomedical Applications. *Molecules* **2022**, *27*, 579, doi:10.3390/molecules27020579.

9. Ashajyothi, C.; Harish, K.H.; Dubey, N.; Chandrakanth, R.K. Antibiofilm activity of biogenic copper and zinc oxide nanoparticles-antimicrobials collegiate against multiple drug resistant bacteria: a nanoscale approach. *J. Nanostructure Chem.* **2016**, *6*, 329–341, doi:10.1007/s40097-016-0205-2.

10. Fahmy, M.D.; Jazayeri, H.E.; Razavi, M.; Hashemi, M.; Omidi, M.; Farahani, M.; Salahinejad, E.; Yadegari, A.; Pitcher, S.; Tayebi, L. Biomedical Applications of Intelligent Nanomaterials. *Intell. Nanomater. Second Ed.* **2016**, *13*, 199–245, doi:10.1002/9781119242628.ch8.

11. Singh, A.; Singh, N.B.; Hussain, I.; Singh, H.; Yadav, V.; Singh, S.C. Green synthesis of nano zinc oxide and evaluation of its impact on germination and metabolic activity of Solanum lycopersicum. *J. Biotechnol.* **2016**, *233*, 84–94, doi:10.1016/j.jbiotec.2016.07.010.

12. Wu, J.; Chen, S.; Ge, S.; Miao, J.; Li, J.; Zhang, Q. Preparation, properties and antioxidant activity of an active film from silver carp (Hypophthalmichthys molitrix) skin gelatin incorporated with green tea extract. *Food Hydrocoll.* **2013**, *32*, 42–51, doi:10.1016/j.foodhyd.2012.11.029.

13. Markova, Z.; Novak, P.; Kaslik, J.; Plachtova, P.; Brazdova, M.; Jancula, D.; Siskova, K.M.; Machala, L.; Marsalek, B.; Zboril, R.; et al. Iron(II,III)-polyphenol complex nanoparticles derived from green tea with remarkable ecotoxicological impact. *ACS Sustain. Chem. Eng.* **2014**, *2*, 1674–1680, doi:10.1021/sc5001435.

14. Nakbanpote, W.; Ruttanakorn, M.; Sukadeetad, K.; Sakkayawong, N.; Damrianant, S. Effects of drying and extraction methods on phenolic compounds and in vitro assays of Eclipta prostrata Linn leaf extracts. *ScienceAsia* **2019**, *45*, 127–137, doi:10.2306/scienceasia1513-1874.2019.45.127.

15. Karam, M.C.; Petit, J.; Zimmer, D.; Baudelaire Djantou, E.; Scher, J. Effects of drying and grinding in production of fruit and vegetable powders: A review. *J. Food Eng.* **2016**, *188*, 32–49, doi:10.1016/j.jfoodeng.2016.05.001.

16. Toropov, N.; Vartanyan, T. Noble Metal Nanoparticles: Synthesis and Optical Properties. *Compr. Nanosci. Nanotechnol.* **2019**, 61–88, doi:10.1016/B978-0-12-803581-8.00585-3.

17. Mohammadi, F.M.; Ghasemi, N. Influence of temperature and concentration on biosynthesis and characterization of zinc oxide nanoparticles using cherry extract. *J. Nanostructure Chem.* **2018**, *8*, 93–102, doi:10.1007/s40097-018-0257-6.

18. Ghodake, G.S.; Deshpande, N.G.; Lee, Y.P.; Jin, E.S. Pear fruit extract-assisted room-temperature biosynthesis of gold nanoplates. *Colloids Surfaces B Biointerfaces* **2010**, *75*, 584–589, doi:10.1016/j.colsurfb.2009.09.040.

19. Zayed, M.F.; Eisa, W.H. Phoenix dactylifera L. leaf extract phytosynthesized gold nanoparticles; controlled synthesis and catalytic activity. *Spectrochim. Acta Part A Mol. Biomol. Spectrosc.* **2014**, *121*, 238–244, doi:10.1016/j.saa.2013.10.092.

20. Gajanan, G.; Chang, M.; Kim, J.; Jin, E. Biogenic materialization using pear extract intended for the synthesis and design of ordered gold nanostructures. *J. Mater. Sci.* **2011**, *46*, 4741–4747, doi:10.1007/s10853-011-5384-0.

21. Rodríguez-Carvajal, J. Recent advances in magnetic structure determination by neutron powder diffraction. *Phys. B Condens. Matter* **1993**, *192*, 55–69, doi:10.1016/0921-4526(93)90108-I.

22. Tran, N.; Mir, A.; Mallik, D.; Sinha, A.; Nayar, S.; Webster, T.J. Bactericidal effect of iron oxide nanoparticles on Staphylococcus aureus. *Int. J. Nanomedicine* **2010**, *5*, 277–283, doi:10.2147/ijn.s9220.

23. Krueger, R.R. Date Palm Status and Perspective in the United States. In *Date Palm Genetic Resources and Utilization*; Springer Netherlands: Dordrecht, 2015; Vol. 2, pp. 447–485 ISBN 9789401796941.

24. Baazaoui, N.; Sghaier-Hammami, B. Green Synthesis of Nanoparticles from Date Palm (Phoenix dactylifera L.). In; Al-Khayri, J.M., Jain, S.M., Johnson, D. V, Eds.; Springer International Publishing: Cham, 2021; pp. 51–69 ISBN 9783030737504.

25. Chao, C.C.T.; Krueger, R.R. The date palm (Phoenix dactylifera L.): Overview of biology, uses, and cultivation. *HortScience* **2007**, *42*, 1077–1082, doi:10.21273/hortsci.42.5.1077.

26. Eddine, L.S.; Segni, L.; Noureddine, G.; Redha, O.M.; Sonia, M. Scavenging Activity, Anti-Inflammatory and Diabetes Related Enzyme Inhibition Properties of Leaves Extract from some Varieties of *Phoenyx dactylifera l. Int. Lett. Chem. Phys. Astron.* **2013**, *14*, 125–135, doi:10.18052/www.scipress.com/ilcpa.14.125.

27. Mohamed, A.; Shafey, E. Green synthesis of metal and metal oxide nanoparticles from plant leaf extracts and their applications: A review. *Green Process. Synth.* **2020**, *9*, 304–339, doi:https://doi.org/10.1515/gps-2020-0031.

28. Jayachandran, A.; T.R., A.; Nair, A.S. Green synthesis and characterization of zinc oxide nanoparticles using Cayratia pedata leaf extract. *Biochem. Biophys. Reports* **2021**, *26*, 100995, doi:10.1016/j.bbrep.2021.100995.

29. Abdullah, J.A.A.; Salah Eddine, L.; Abderrhmane, B.; Alonso-González, M.; Guerrero, A.; Romero, A.; Ahmed, J.A.; Salah, L.; Abderrhmane, B. Green synthesis and characterization of iron oxide nanoparticles by pheonix dactylifera leaf extract and evaluation of their antioxidant activity. *Sustain. Chem. Pharm.* **2020**, *17*, 100280, doi:10.1016/j.scp.2020.100280.

30. Abdullah, J.A.A.; Jiménez-Rosado, M.; Perez-Puyana, V.; Guerrero, A.; Romero, A. Green Synthesis of FexOy Nanoparticles with Potential Antioxidant Properties. *Nanomaterials* **2022**, *12*, 2449, doi:10.3390/nano12142449.

31. Barzinjy, A.A.; Azeez, H.H. Green synthesis and characterization of zinc oxide nanoparticles using Eucalyptus globulus Labill. leaf extract and zinc nitrate hexahydrate salt. *SN Appl. Sci.* **2020**, *2*, 1–14, doi:10.1007/s42452-020-2813-1.

32. Bibi, I.; Kamal, S.; Ahmed, A.; Iqbal, M.; Nouren, S.; Jilani, K.; Nazar, N.; Amir, M.; Abbas, A.; Ata, S.; et al. Nickel nanoparticle synthesis using Camellia Sinensis as reducing and capping agent: Growth mechanism and photo-catalytic activity evaluation. *Int. J. Biol. Macromol.* **2017**, *103*, 783–790, doi:10.1016/j.ijbiomac.2017.05.023.

33. Ayachi, A.A.; Mechakra, H.; Silvan, M.M.; Boudjaadar, S.; Achour, S. Monodisperse α-Fe2O3 nanoplatelets: Synthesis and characterization. *Ceram. Int.* **2015**, *41*, 2228–2233, doi:10.1016/j.ceramint.2014.10.024.

34. Behera, S.S.; Patra, J.K.; Pramanik, K.; Panda, N.; Thatoi, H. Characterization and Evaluation of Antibacterial Activities of Chemically Synthesized Iron Oxide Nanoparticles. *World J. Nano Sci. Eng.* **2012**, *02*, 196–200, doi:10.4236/wjnse.2012.24026.

35. Abdullah, J.A.A.; Jiménez-Rosado, M.; Guerrero, A.; Romero, A. Gelatin-Based Biofilms with FexOy-NPs Incorporated for Antioxidant and Antimicrobial Applications. *Materials (Basel).* **2022**, *15*, 1966, doi:10.3390/ma15051966.

36. Albertsson, J.; Abrahams, S.C.; Kvick, Å. Atomic displacement, anharmonic thermal vibration, expansivity and pyroelectric coefficient thermal dependences in ZnO. *Acta Crystallogr. Sect. B Struct. Sci.* **1989**, *45*, 34–40, doi:10.1107/S0108768188010109.

37. Park, J.H.; Park, C.; Lee, K.S.; Suh, S.J. Effect of NaOH and precursor concentration on size and magnetic properties of FeCo nanoparticles synthesized using the polyol method. *AIP Adv.* **2020**, *10*, doi:10.1063/5.0024622.

38. Kim, H. seok; Seo, Y.S.; Kim, K.; Han, J.W.; Park, Y.; Cho, S. Concentration Effect of Reducing Agents on Green Synthesis of Gold Nanoparticles: Size, Morphology, and Growth Mechanism. *Nanoscale Res. Lett.* **2016**, *11*, doi:10.1186/s11671-016-1393-x.

39. Suresh, D.; Nethravathi, P.C.; Udayabhanu; Pavan Kumar, M.A.; Raja Naika, H.; Nagabhushana, H.; Sharma, S.C. Chironji mediated facile green synthesis of ZnO nanoparticles and their photoluminescence, photodegradative, antimicrobial and antioxidant activities. *Mater. Sci. Semicond. Process.* **2015**, *40*, 759–765, doi:10.1016/j.mssp.2015.06.088.

40. Wang, X.; Yang, D.P.; Huang, P.; Li, M.; Li, C.; Chen, D.; Cui, D. Hierarchically assembled Au microspheres and sea urchin-like architectures: Formation mechanism and SERS study. *Nanoscale* **2012**, *4*, 7766–7772, doi:10.1039/c2nr32405a.

41. Fuad, A.; Fibriyanti, A.A.; Subakti; Mufti, N.; Taufiq, A. Effect of Precursor Concentration Ratio on the Crystal Structure, Morphology, and Band Gap of ZnO Nanorods. *IOP Conf. Ser. Mater. Sci. Eng.* **2017**, *202*, doi:10.1088/1757-899X/202/1/012074.

42. Jon, R.; Martin, N.; Dasari, P.R.; Paul, A.; Singh, V. Effect of Physical Parameters on Green Synthesis of Gold Nanoparticles using Zea Mays Extract. *Int. J. Eng. Adv. Technol.* **2019**, *9*, 870–873, doi:10.35940/ijeat.f8819.129219.

43. Hosseini Largani, S.; Akbarzadeh Pasha, M. The effect of concentration ratio and type of functional group on synthesis of CNT–ZnO hybrid nanomaterial by an in situ sol–gel process. *Int. Nano Lett.* **2017**, *7*, 25–33, doi:10.1007/s40089-016-0197-4.

44. Singh, J.; Dutta, T.; Kim, K.-H.; Rawat, M.; Samddar, P.; Kumar, P. 'Green' synthesis of metals and their oxide nanoparticles: applications for environmental remediation. *J. Nanobiotechnology* **2018**, *16*, 84, doi:10.1186/s12951-018-0408-4.

45. Mukunthan, K.S.; Balaji, S. Cashew Apple Juice (Anacardium occidentale L.) Speeds Up the Synthesis of Silver Nanoparticles. *Int. J. Green Nanotechnol.* **2012**, *4*, 71–79, doi:10.1080/19430892.2012.676900.

46. Love, A.J.; Makarov, V. V.; Sinitsyna, O. V.; Shaw, J.; Yaminsky, I. V.; Kalinina, N.O.; Taliansky, M.E. A Genetically Modified Tobacco Mosaic Virus that can Produce Gold Nanoparticles from a Metal Salt Precursor. *Front. Plant Sci.* **2015**, *6*, doi:10.3389/fpls.2015.00984.

47. Vega-Poot, A.G.; Rodríguez-Gattorno, G.; Soberanis-Domínguez, O.E.; Patiño-Díaz, R.T.; Espinosa-Pesqueira, M.; Oskam, G. The nucleation kinetics of ZnO nanoparticles from ZnCl2 in ethanol solutions. *Nanoscale* **2010**, *2*, 2710–2717, doi:10.1039/c0nr00439a.

48. Andarini, N.; Farida, R.S.; Haryati, T. The Effect of Different Precursor Concentration on The Synthesis of CaO Nanoparticles with Coprecipitation Methods for Palm Oil Transesterification Catalysis. *Reaktor* **2021**, *21*, 45–51, doi:10.14710/reaktor.21.2.45-51.

49. Shokry Hassan, H.; Kashyout, A.B.; Soliman, H.M.A.; Uosif, M.A.; Afify, N. Influence of Reaction Time , Reducing Agent and Zinc Precursors on the Morphological Structures of Zinc Oxide. *Hurghada – Egypt* **2013**.

50. Pudukudy, M.; Yaakob, Z. Facile Synthesis of Quasi Spherical ZnO Nanoparticles with Excellent Photocatalytic Activity. *J. Clust. Sci.* **2015**, *26*, 1187–1201, doi:10.1007/s10876-014-0806-1.

51. Soto-Robles, C.A.; Luque, P.A.; Gómez-Gutiérrez, C.M.; Nava, O.; Vilchis-Nestor, A.R.; Lugo-Medina, E.; Ranjithkumar, R.; Castro-Beltrán, A. Study on the effect of the concentration of Hibiscus sabdariffa extract on the green synthesis of ZnO nanoparticles. *Results Phys.* **2019**, *15*, doi:10.1016/j.rinp.2019.102807.

52. Sibiya, P.N.; Moloto, M.J. Effect of precursor concentration and pH on the shape and size of starch capped silver selenide (Ag2Se) nanoparticles. *Chalcogenide Lett.* **2014**, *11*, 577–588.

53. Junaid, M.; Dowlath, H.; Anjum, S.; Khalith, S.B.M.; Varjani, S.; Kumar, S.; Munuswamy, G.; Woong, S.; Jin, W.; Ravindran, B. Comparison of characteristics and biocompatibility of green synthesized iron oxide nanoparticles with chemical synthesized nanoparticles. *Environ. Res.* **2021**, *201*, 111585, doi:10.1016/j.envres.2021.111585.

54. Hsu, C.-M.; Huang, Y.-H.; Chen, H.-J.; Lee, W.-C.; Chiu, H.-W.; Maity, J.P.; Chen, C.-C.; Kuo, Y.-H.; Chen, C.-Y. Green synthesis of nano-Co3O4 by Microbial Induced Precipitation (MIP) process using Bacillus pasteurii and its application as supercapacitor. *Mater. Today Commun.* **2018**, *14*, 302–311, doi:10.1016/j.mtcomm.2018.02.005.

55. Wang, T.; Jin, X.; Chen, Z.; Megharaj, M.; Naidu, R. Science of the Total Environment Green synthesis of Fe nanoparticles using eucalyptus leaf extracts for treatment of eutrophic wastewater. *Sci. Total Environ.* **2014**, *466–467*, 210–213, doi:10.1016/j.scitotenv.2013.07.022.

56. Udvardi, B.; Kovács, I.J.; Fancsik, T.; Kónya, P.; Bátori, M.; Stercel, F.; Falus, G.; Szalai, Z. Effects of Particle Size on the Attenuated Total Reflection Spectrum of Minerals. *Appl. Spectrosc.* **2017**, *71*, 1157–1168, doi:10.1177/0003702816670914.

57. Mohan Kumar, K.; Mandal, B.K.; Siva Kumar, K.; Sreedhara Reddy, P.; Sreedhar, B. Biobased green method to synthesise palladium and iron nanoparticles using Terminalia chebula aqueous extract. *Spectrochim. Acta Part A Mol. Biomol. Spectrosc.* **2013**, *102*, 128–133, doi:10.1016/j.saa.2012.10.015.

58. Salgado, P.; Márquez, K.; Rubilar, O.; David Contreras, ·; Vidal, G. The effect of phenolic compounds on the green synthesis of iron nanoparticles (Fe x O y-NPs) with photocatalytic activity. *Appl. Nanosci.* **2019**, *9*, 371–385, doi:10.1007/s13204-018-0931-5.

59. Keshari, A.K.; Srivastava, R.; Singh, P.; Yadav, V.B.; Nath, G. Antioxidant and antibacterial activity of silver nanoparticles synthesized by Cestrum nocturnum. *J. Ayurveda Integr. Med.* **2020**, *11*, 37–44, doi:10.1016/j.jaim.2017.11.003.

60. Demirbas, A.; Welt, B.A.; Ocsoy, I. Biosynthesis of red cabbage extract directed Ag NPs and their effect on the loss of antioxidant activity. *Mater. Lett.* **2016**, *179*, 20–23, doi:10.1016/j.matlet.2016.05.056.

61. Zhao, X.; Zhou, L.; Shahid, M.; Rajoka, R.; Yan, L.; Shao, D.; Zhu, J.; Shi, J.; Huang, Q.; Yang, H. Critical Reviews in Biotechnology Fungal silver nanoparticles : synthesis , application and challenges. *Crit. Rev. Biotechnol.* **2018**, *38*, 817–835, doi:10.1080/07388551.2017.1414141.

62. Öztürk, F.; Ço, S.; Duman, F. Materials Science & Engineering C Biosynthesis of silver nanoparticles using leaf extract of Aesculus hippocastanum (horse chestnut): Evaluation of their antibacterial , antioxidant and drug release system activities. **2020**, *107*, doi:10.1016/j.msec.2019.110207.

63. Bedlovičová, Z.; Strapáč, I.; Baláž, M.; Salayová, A. A brief overview on antioxidant activity determination of silver nanoparticles. *Molecules* **2020**, *25*, 1–24, doi:10.3390/molecules25143191.

64. Myint, K. zar; Yu, Q.; Xia, Y.; Qing, J.; Zhu, S.; Fang, Y.; Shen, J. Bioavailability and antioxidant activity of nanotechnology-based botanic antioxidants. *J. Food Sci.* **2021**, *86*, 284–292, doi:10.1111/1750-3841.15582.

65. Pu, S.; Li, J.; Sun, L.; Zhong, L.; Ma, Q. An in vitro comparison of the antioxidant activities of chitosan and green synthesized gold nanoparticles. *Carbohydr. Polym.* **2019**, *211*, 161–172, doi:10.1016/j.carbpol.2019.02.007.

66. Armijo, L.M.; Wawrzyniec, S.J.; Kopciuch, M.; Brandt, Y.I.; Rivera, A.C.; Withers, N.J.; Cook, N.C.; Huber, D.L.; Monson, T.C.; Smyth, H.D.C.; et al. Antibacterial activity of iron oxide, iron nitride, and tobramycin conjugated nanoparticles against Pseudomonas aeruginosa biofilms. *J. Nanobiotechnology* **2020**, *18*, 1–27, doi:10.1186/s12951-020-0588-6.

67. Lee, C.; Jee, Y.K.; Won, I.L.; Nelson, K.L.; Yoon, J.; Sedlak, D.L. Bactericidal effect of zero-valent iron nanoparticles on Escherichia coli. *Environ. Sci. Technol.* **2008**, *42*, 4927–4933, doi:10.1021/es800408u.

68. Mahdy, S.A.; Raheed, Q.J.; Kalaichelvan, P.T. Antimicrobial activity of zero-valent iron nanoparticles. *Int. J. Mod. Eng. Res. www.ijmer.com* **2012**, *2*, 578–581.

69. Touati, D. Iron and Oxidative Stress in Bacteria. *Arch. Biochem. Biophys.* **2000**, *373*, 1–6, doi:10.1006/abbi.1999.1518.

70. Datta, A.; Patra, C.; Bharadwaj, H.; Kaur, S.; Dimri, N.; Khajuria, R. Green Synthesis of Zinc Oxide Nanoparticles Using Parthenium hysterophorus Leaf Extract and Evaluation of their Antibacterial Properties. *J. Biotechnol. Biomater.* **2017**, *07*, 3–7, doi:10.4172/2155-952x.1000271.

71. Awwad, A.M.; Amer, M.W. Biosynthesis of copper oxide nanoparticles using Ailanthus altissima leaf extract and antibacterial activity. *Chem. Int.* **2020**, *6*, 210–2017.

72. Mohan, P.; Mala, R. Comparative antibacterial activity of magnetic iron oxide nanoparticles synthesized by biological and chemical methods against poultry feed pathogens. *Mater. Res. Express* **2019**, *6*, doi:10.1088/2053-1591/ab4964.

73. Shuai, C.; Wang, C.; Qi, F.; Peng, S.; Yang, W.; He, C.; Wang, G.; Qian, G. Enhanced Crystallinity and Antibacterial of PHBV Scaffolds Incorporated with Zinc Oxide. *J. Nanomater.* **2020**, *2020*, 1–12, doi:10.1155/2020/6014816.

Tables

Table 1: Results obtained for different parameters of the ZnO-NPs synthesized using Phoenix dactylifera L. extract at different ratios ([1:1], [1:2] and [2:1]) and concentrations (0.1, 0.2, 0.4, 0.5, 1 and 2 M): average diameter in nm (from DRX measurements, TEM and SEM images), average length in nm (from SEM), crystallinity percentage, and antioxidant activity (IC50 DPPH free radical in mg/mL and TAC in mgGAE/mg ZnO-NPs-NPs).

Ratio	$ZnCl_2$: Ext [M]	D DRX (nm)	D TEM (nm)	D SEM (nm)	Length (nm)	Crystallinity %	TAC (mgGAE/mg NPs)	IC_{50} (mg/ml)
2:1	0.2:0.1	19.7 ± 1.2^{i}	18.6 ± 0.5^{h}	18.1 ± 0.5^{i}	108 ± 33^{cd}	83.5^{h}	4.1 ± 0.0^{ab}	2.04 ± 0.1^{e}
	0.5:0.25	31.4 ± 1.4^{f}	30.1 ± 0.3^{e}	31.5 ± 0.3^{f}	216 ± 107^{ab}	86.3^{f}	1.1 ± 0.1^{c}	4.24 ± 0.1^{d}
	1:0.5	38.4 ± 1.0^{d}	39.0 ± 0.1^{c}	38.3 ± 0.6^{d}	197 ± 56^{bc}	89.0^{d}	0.5 ± 0.0^{c}	5.20 ± 0.3^{b}
1:1	0.2:0.2	26.7 ± 0.1^{h}	19.8 ± 0.2^{g}	25.1 ± 0.8^{h}	151 ± 22^{bc}	83.6^{i}	2.3 ± 1.6^{bc}	1.38 ± 0.0^{f}
	0.5:0.5	36.4 ± 0.6^{e}	37.3 ± 0.4^{d}	36.8 ± 0.9^{e}	291 ± 37^{a}	87.0^{e}	1.6 ± 0.1^{c}	4.83 ± 0.3^{c}
	1:1	44.3 ± 0.5^{b}	41.6 ± 0.9^{b}	46 ± 0.7^{b}	219 ± 31^{ab}	92.8^{b}	1.4 ± 1.9^{c}	6.77 ± 0.3^{a}
1:2	0.2:0.4	28.3 ± 0.9^{g}	28.5 ± 0.8^{f}	28.7 ± 0.6^{g}	48 ± 15^{d}	84.2^{g}	1.3 ± 0.1^{c}	1.17 ± 0.1^{f}
	0.5:1	41.2 ± 1.2^{c}	40.0 ± 0.1^{c}	40.4 ± 1.4^{c}	109 ± 36^{cd}	92.2^{c}	$2.7 \pm 2.4b^{c}$	2.07 ± 0.1^{e}
	1:2	49.8 ± 1.7^{a}	61.6 ± 1.3^{a}	49.6 ± 0.3^{a}	120 ± 42^{cd}	93.2^{a}	5.4 ± 0.4^{a}	2.17 ± 0.1^{e}

Note: Different superscript letters (a–i) within a column indicate significant differences among mean observations ($p < 0.05$).

Table 2: The inhibition zones (represented by their diameter in mm) produced by green synthesized ZnO-NPs against Staphylococcus aureus (S. aureus) and Escherichia coli (E. coli). Gentamicin was used as a standard.

Test time (h)	Samples		Inhibition diameter (mm)	
			Staphylococcus aureus	Escherichia coli
24	1	Gentamicin	28.3 ± 0.3^{a}	30.4 ± 0.7^{A}
	2	ZnO-NPs [0.2:0.1]	19.4 ± 0.2^{b}	21 ± 0.4^{B}
	3	ZnO-NPs [0.2:04]	18.2 ± 0.2^{c}	19.2 ± 0.6^{C}
48	1	Gentamicin	26.6 ± 0.1^{a}	28.1 ± 0.4^{A}
	2	ZnO-NPs [0.2:0.1]	17.7 ± 0.2^{b}	17.4 ± 0.7^{B}
	3	ZnO-NPs [0.2:04]	17.0 ± 0.1^{c}	16.4 ± 0.5^{B}
Note: Different superscript letters (a–c and A-B) within a column in a time raw indicate significant differences among mean observations ($p < 0.05$).				

Figures

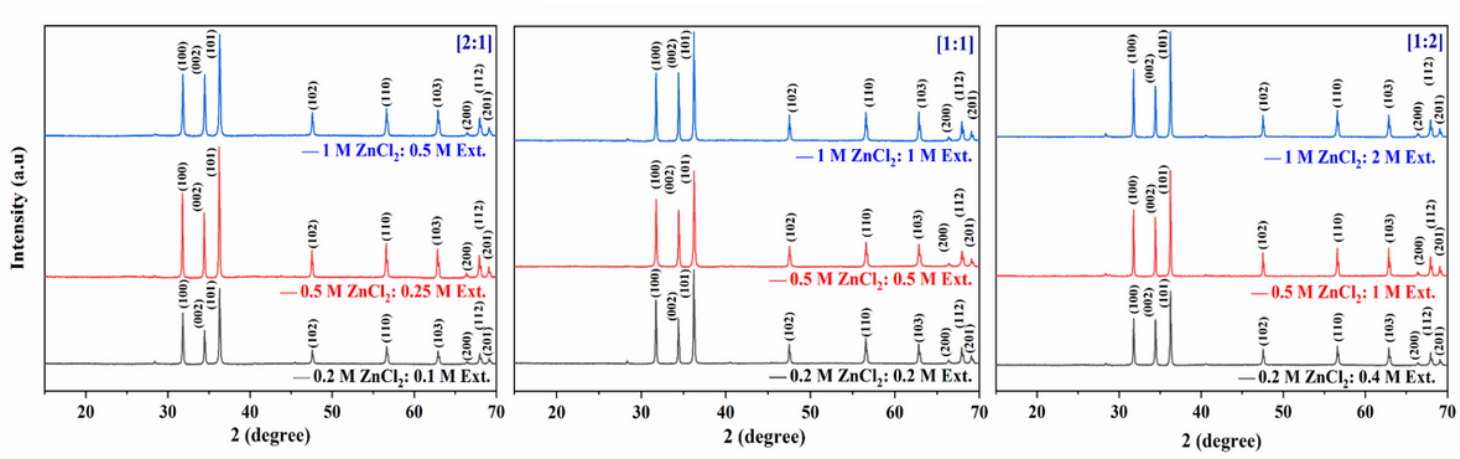

Figure 1

Mechanism for the green synthesis of ZnO nanoparticles.

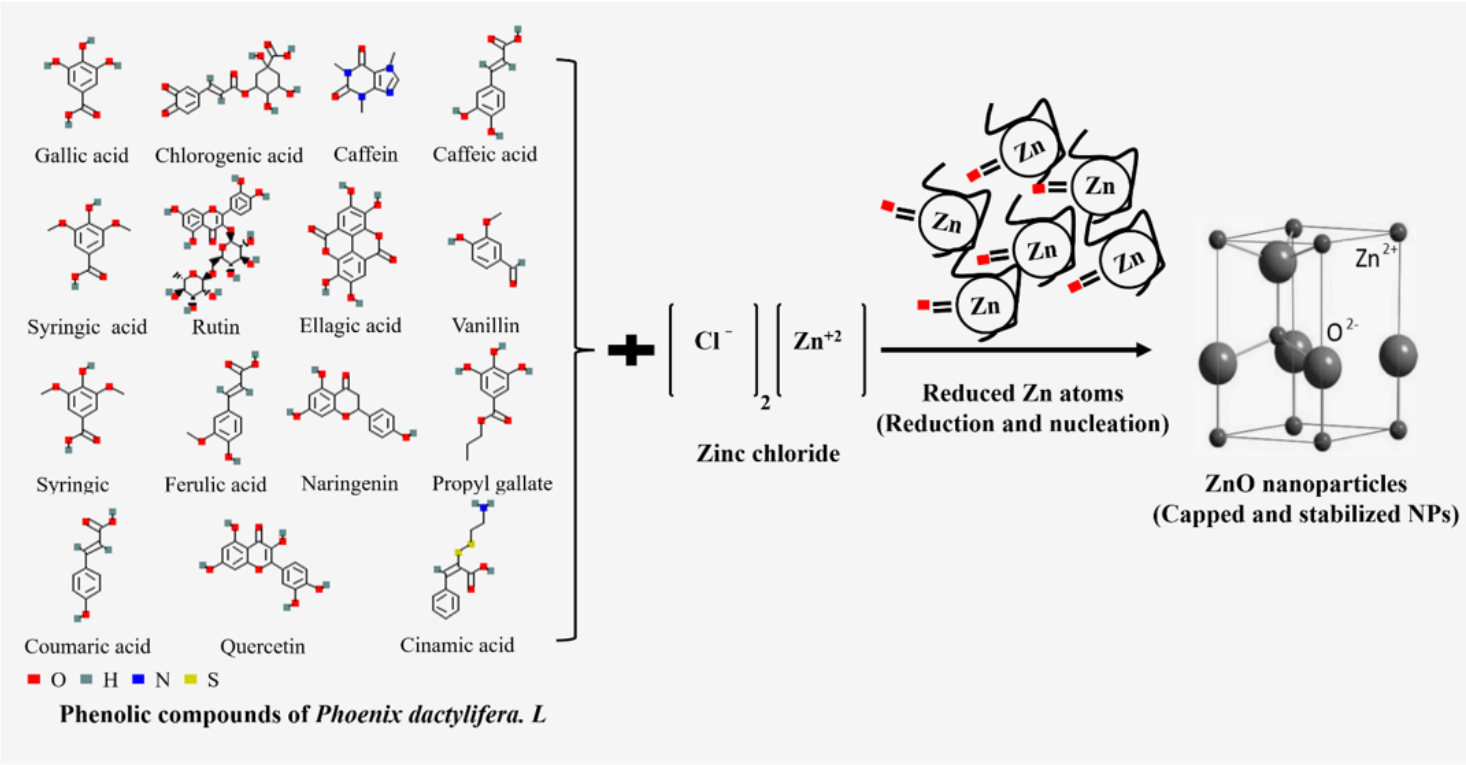

Figure 2

XRD spectrum of the ZnO-NPs (JCPDS standard) synthesized using Phoenix dactylifera L. extract at different ratios ([1:1], [1:2] and [2:1]) and concentrations (0.1, 0.2, 0.4, 0.5, 1 and 2 M).

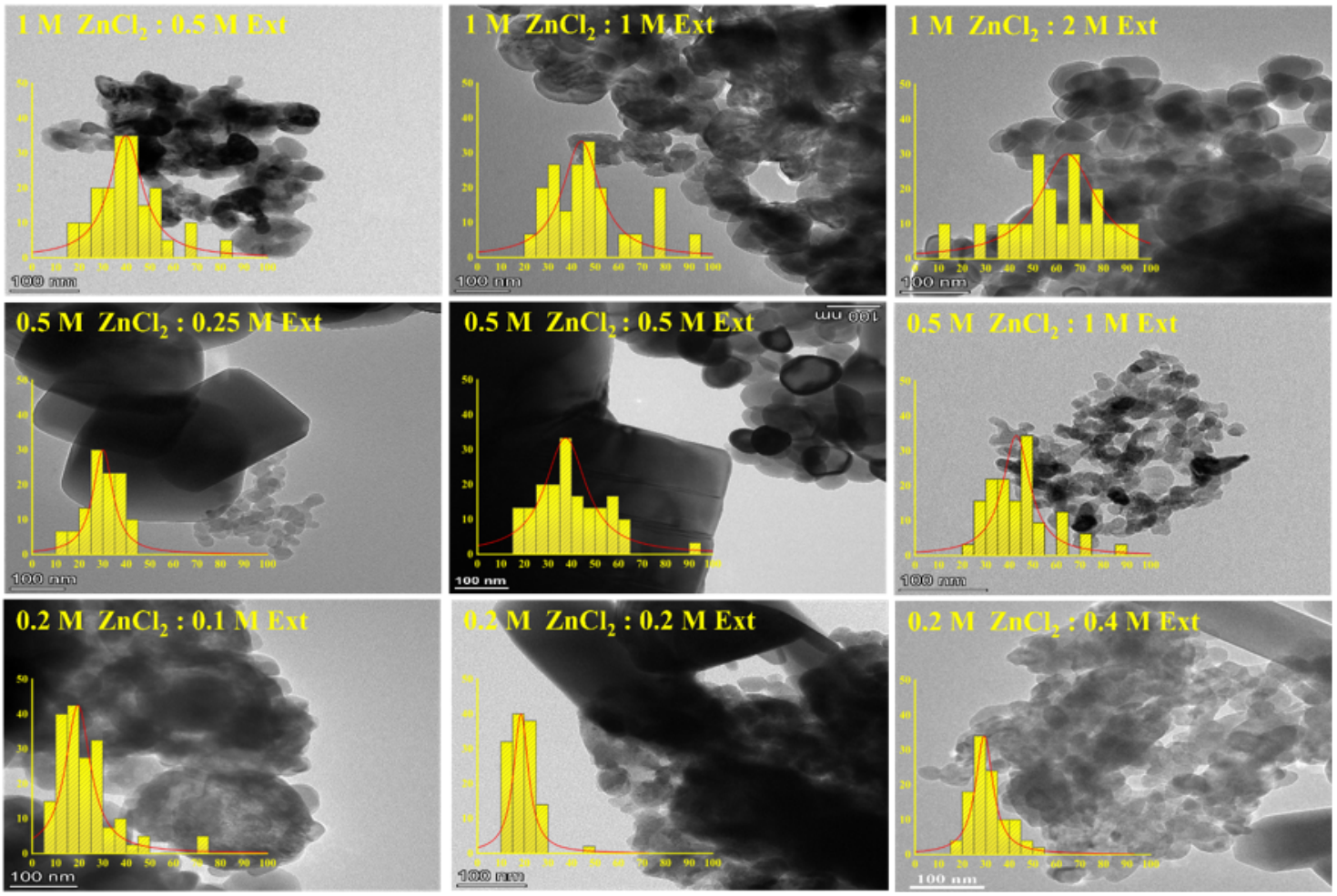

Figure 3

Transmission electron microscopy (TEM) images of ZnO-NPs synthesized using Phoenix dactylifera L. extract at different ratios ([1:1], [1:2] and [2:1]) and concentrations (0.1, 0.2, 0.4, 0.5, 1 and 2 M).

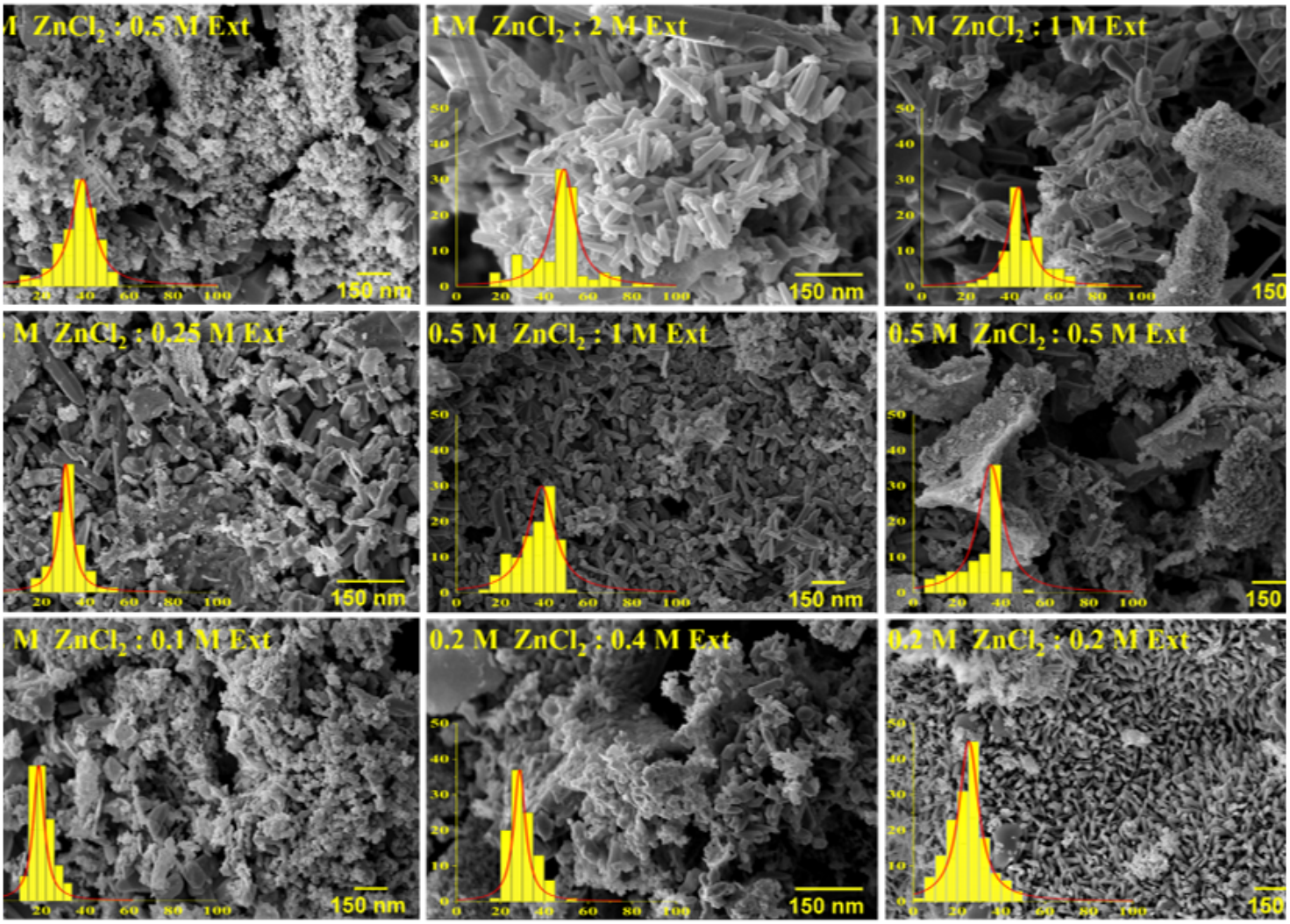

Figure 4

Scanning electron microscopy (SEM) images of ZnO-NPs synthesized using Phoenix dactylifera L. extract at different ratios ([1:1], [1:2] and [2:1]) and concentrations (0.1, 0.2, 0.4, 0.5, 1 and 2 M).

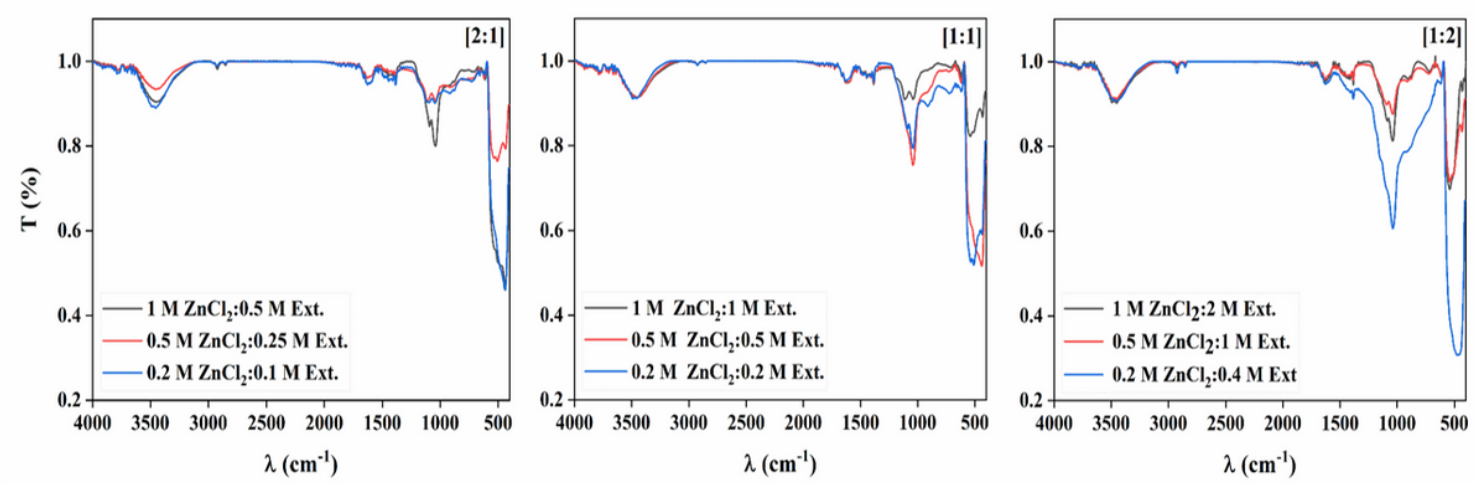

Figure 5

FTIR spectrum of the ZnO-NPs synthesized using Phoenix dactylifera L.extract at different ratios ([1:1], [1:2] and [2:1]) and concentrations (0.1, 0.2, 0.4, 0.5, 1 and 2 M).

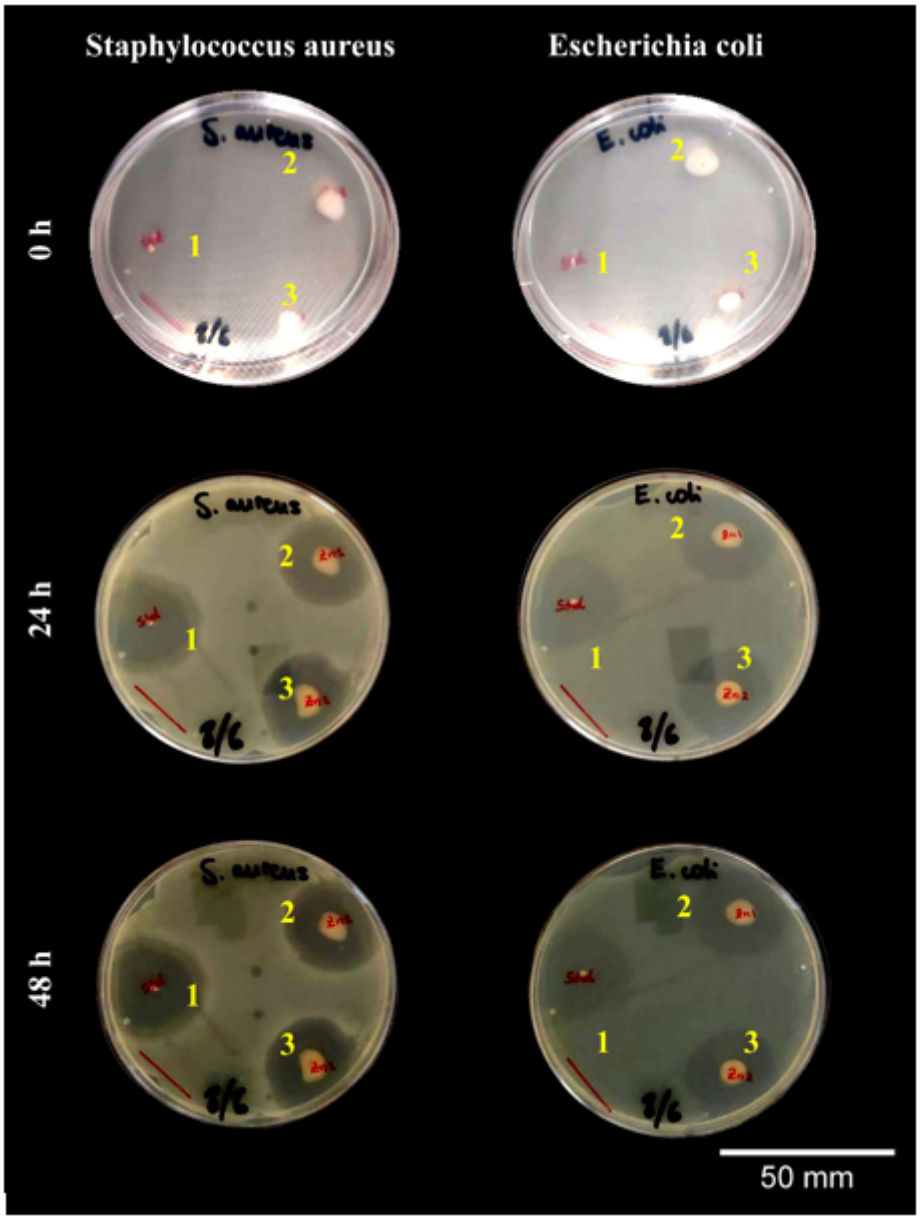

Figure 6

Image of inhibition area over time produced by green synthesized ZnO-NPs against Staphylococcus aureus (S. aureus) and Escherichia coli (E. coli). Gentamicin was used as a standard.